Title

Evidence that Criegee intermediates drive autoxidation in unsaturated lipids

Journal

Proceedings of the National Academy of Sciences of the United States of America, 117(9)

ISSN

0027-8424

Authors

Zeng, Meirong

Heine, Nadja

Wilson, Kevin R

Publication Date

2020-03-03

DOI

10.1073/pnas.1920765117

Peer reviewed

Evidence that Criegee intermediates drive autoxidation in unsaturated lipids

Meirong Zeng[a], Nadja Heine[a], and Kevin R. Wilson[a,1]

[a]Chemical Sciences Division, Lawrence Berkeley National Laboratory, Berkeley, CA 94720

Edited by Barbara J. Finlayson-Pitts, University of California, Irvine, CA, and approved January 22, 2020 (received for review November 25, 2019)

Autoxidation is an autocatalytic free-radical chain reaction responsible for the oxidative destruction of organic molecules in biological cells, foods, plastics, petrochemicals, fuels, and the environment. In cellular membranes, lipid autoxidation (peroxidation) is linked with oxidative stress, age-related diseases, and cancers. The established mechanism of autoxidation proceeds via H-atom abstraction through a cyclic network of peroxy–hydroperoxide-mediated free-radical chain reactions. For a series of model unsaturated lipids, we present evidence for an autoxidation mechanism, initiated by hydroxyl radical (OH) addition to C=C bonds and propagated by chain reactions involving Criegee intermediates (CIs). This mechanism leads to unexpectedly rapid autoxidation even in the presence of water, implying that as reactive intermediates, CI could play a much more prominent role in chemistries beyond the atmosphere.

autoxidation | Criegee intermediate | unsaturated lipids

As a consequence of the Earth's oxygen-rich atmosphere, reactive oxygen species (ROS) are formed ubiquitously during photochemistry, pollution events, smoking, and in vivo during cellular respiration and as byproducts of biochemical pathways (1, 2). ROS include hydroxyl (OH) and hydroperoxyl radicals (HO_2), hydrogen peroxide (H_2O_2), superoxide, and excited states of O_2. ROS degrade organic molecules by initiating and propagating free-radical chain reactions known as autoxidation (3). In cells, autoxidation of lipids, known as peroxidation (3), disrupts membrane structure and function and induces oxidative stress and rancidity in foods. Oxidative stress (3, 4) is widely implicated in aging, cancer, neurodegeneration, diabetes, and so on (5, 6). Substantial commercial effort is devoted to antioxidant formulations to short-circuit autoxidation to prevent disease and prolong the shelf life of foods, plastics, and other industrial products (7). Rational design of antioxidants in turn depends upon understanding the rates, mechanisms, and intermediates involved in autoxidation.

Autoxidation (i.e., lipid peroxidation) is a free-radical chain reaction that occurs in three phases: initiation, propagation, and termination (3). For lipids that contain C=C bonds, evidence gathered since the 1940s shows that autoxidation is initiated via H abstraction by ROS and other radicals at allylic and biallylic reaction sites (8, 9). Propagation occurs via H-atom transfer to peroxy radicals (RO_2) to form hydroperoxides (ROOH), which maintains the radical pool (Fig. 1*A*). Decomposition and further reactions of ROOH form additional radical products that amplify the chain reaction. However, a number of studies report reaction products (e.g., epoxides and various scission products) that are not easily explained by this established mechanism (Fig. 1*A*), suggesting that other reaction networks are involved (10, 11). Here, we present evidence for an additional autoxidation mechanism initiated by OH addition to C=C bonds and propagated by pathways involving Criegee intermediates (CIs).

Previous mechanistic studies of lipid peroxidation were typically initiated by azo compounds (3, 12) to mimic the role of ROS, which are difficult to study due to their high reactivity and complex kinetics. The use of azo initiators, as ROS proxies, preselects the main autoxidation pathways to proceed via the established H abstraction route shown in Fig. 1*A*. Thus for OH, which can both rapidly abstract H atoms as well as add to C=C double bonds (13), azo initiators may not always capture the operative pathways in the environment or in biology.

The hydroxyl radical (OH) is readily formed in the environment/atmosphere photochemically (1) and in vivo (2). Despite its substantial reactivity toward all major classes of biological molecules, very few studies have focused on isolating OH reactivity from other ROS (14). Early studies suggest that the reaction mechanism of OH with unsaturated lipids might be rather different from other ROS species (13).

The OH-initiated autoxidation of model liquid-phase lipids is examined using a continuous flow stirred tank reactor (15). Lipid nanodroplets are introduced as aerosols and exposed to gas-phase OH, produced in situ (*Methods*). Reaction kinetics and products are measured in real time using a vacuum UV aerosol mass spectrometer (16, 17). This approach differs substantially from previous experiments but is designed to achieve controlled and quantifiable OH initiation and propagation rates. This is done by precisely measuring the gas-phase OH concentration ([OH]) and droplet surface area, which together yield, via gas kinetic theory, a precise measure of the OH-droplet collision frequency (i.e., initiation rate). From the OH collision frequency and consumption rate of the lipid, an effective reaction probability (γ_{eff}) can be determined (15). γ_{eff} is the fraction of OH collisions that yield a reaction. If the lipid is consumed at or near the OH collision frequency, then $\gamma_{eff} \leq 1$, whereas values larger than 1 indicate the presence of free-radical chain reactions (i.e., autoxidation) (18, 19).

Using this approach, the OH reaction kinetics and products were measured for a series of neat model lipid compounds: squalene (Sqe, $C_{30}H_{50}$), arachidonic acid (AA, $C_{20}H_{32}O_2$), linoleic acid

Significance

Autoxidation leads to the slow persistent destruction of organic molecules causing oxidative stress and associated disease. The prevailing autoxidation mechanism of unsaturated lipids involves chain reactions initiated and propagated by H-atom abstraction, mediated by peroxy radicals and other reactive oxygen species. Here we report experimental evidence for an autoxidation mechanism initiated by OH, which is unanticipated and proceeds by OH addition followed by pathways involving Criegee intermediates (CIs). Although CIs are routinely encountered in atmospheric and synthetic organic chemistry, their role in autoxidation is unexpected. Our results suggest that in all likelihood these exotic species play a much more prominent and general role in the chemistry of cells, food, petrochemicals, and the environment beyond what is currently believed.

Author contributions: M.Z. and K.R.W. designed research; M.Z. and N.H. performed research; M.Z. analyzed data; and M.Z., N.H., and K.R.W. wrote the paper.

The authors declare no competing interest.

This article is a PNAS Direct Submission.

[1]To whom correspondence may be addressed. Email: KRWilson@lbl.gov.

This article contains supporting information online at https://www.pnas.org/lookup/suppl/doi:10.1073/pnas.1920765117/-/DCSupplemental.

First published February 18, 2020.

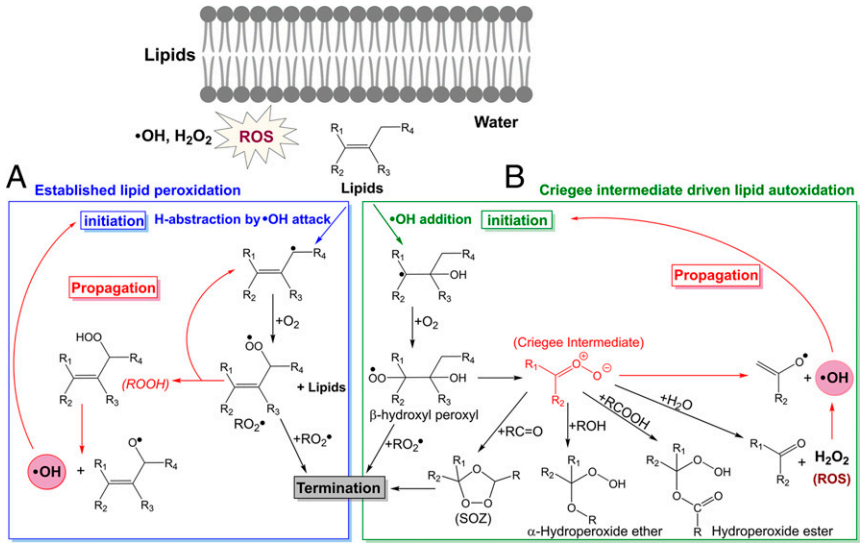

Fig. 1. Two reaction schemes for the OH-initiated autoxidation of unsaturated lipids. (*A*) The established lipid peroxidation scheme, which is initiated by H abstraction at allylic C-H sites and propagated by peroxy radicals (RO_2) and hydroperoxides (ROOH). (*B*) CI-driven lipid autoxidation mechanism, which is initiated by the OH addition reactions and propagated by chain reactions involving the CI. The reaction of two RO_2 radicals are common termination steps in both mechanisms. Additional termination reactions of CI include their reactions with aldehydes (RC = O) to produce SOZs, with alcohols (ROH) to produce α-hydroperoxide ethers, and with carboxylic acids (ROOH) to produce hydroperoxide esters.

(LA, $C_{18}H_{32}O_2$), oleic acid (OA, $C_{18}H_{34}O_2$), and cis-9-tricosene (Tri, $C_{23}H_{46}$). Sqe is a major constituent (~12%) in human sebum (20), while AA, LA, and OA are important unsaturated fatty acid components of phospholipid cell membranes (3). These compounds differ in the number of C=C, allylic and biallylic C–H bonds, and functional groups enabling insight into how molecular structure alters autoxidation rates and product distributions (3).

Shown in Fig. 2 is γ_{eff} as a function of [OH] for Sqe, AA, LA, OA, and Tri. [OH] is kept low to mimic environmental and biological conditions where autoxidation occurs. For those molecules with C=C bonds, $\gamma_{eff} > 1$. For Sqe, at [OH] ~10^6 cm^{-3}, γ_{eff} approaches ~70, indicating that for every OH collision, 70 Sqe molecules are additionally consumed by radical chain cycling pathways. At [OH] ~10^7 cm^{-3}, γ_{eff} is around 21, 31, 8, 6, and 3 for Sqe, AA, LA, OA, and Tri, respectively. γ_{eff} is observed to increase with the number of C=C bonds with the exception of AA, which exhibits a slightly larger reactivity than that of Sqe despite having two fewer C=C bonds. This trend points to the key role that C=C bond number plays both in the initiation and propagation steps, as discussed below.

For the unsaturated lipids, decreasing [OH] increases γ_{eff}, providing clear evidence for radical cycling (i.e., autoxidation), since higher [OH] produces a larger radical density in the droplet, which favors radical + radical termination reactions (e.g., RO_2 + RO_2, Fig. 1) (18). In contrast, radical chain cycling is not observed ($\gamma_{eff} < 1$) for three saturated compounds: squalane (Sqa, no C=C double bonds, $\gamma_{eff} \sim 0.5$) (15), 2-octyl-1-dodecanol ($\gamma_{eff} \sim 0.2$), and 2-decyl-tetradecanol ($\gamma_{eff} \sim 0.3$).

While the observations in Fig. 2 confirm that autoxidation occurs and is consistent with previous studies, the major lipid reaction products that are detected are not. Shown in Fig. 3 is a mass spectrum recorded for Sqe ($m/z = 410$) during the OH reaction. A series of peaks are observed at m/z = 248, 316, and 384 and are identified as aldehydes ($C_{17}H_{28}O$, $C_{22}H_{36}O$, and $C_{27}H_{44}O$). Other reaction products are observed at m/z = 322, 390, 458, 526, and 594 and are identified as secondary ozonides (SOZs). The observation of SOZs is unexpected and together with the aldehydes are nearly identical to the products typically observed in alkene ozonolysis reactions. For example, the ozonolysis of Sqe (21) produces the same five SOZs (*SI Appendix*, Fig. S3), which are formed by reactions of CIs with carbonyl compounds (21, 22). Extensive experimental checks confirmed that the ozone concentration in our reactor is below 1–3 ppb and therefore too small to account for the observed products (*SI Appendix*, Fig. S1). Thus, the detection of SOZs, instead of hydroperoxides (ROOH, Fig. 1*A*), formed by OH autoxidation provides a distinctive fingerprint for the presence of CI. This is consistent with recent observations by Beauchamp and coworkers (23), who reported evidence for CI formed during OH reactions.

As further confirmation for the presence of CI, two liquid alcohols (2-octyl-1-dodecanol and 2-decyl-1-tetradecanol) were separately added to the nanodroplets comprising Sqe (Fig. 3 and

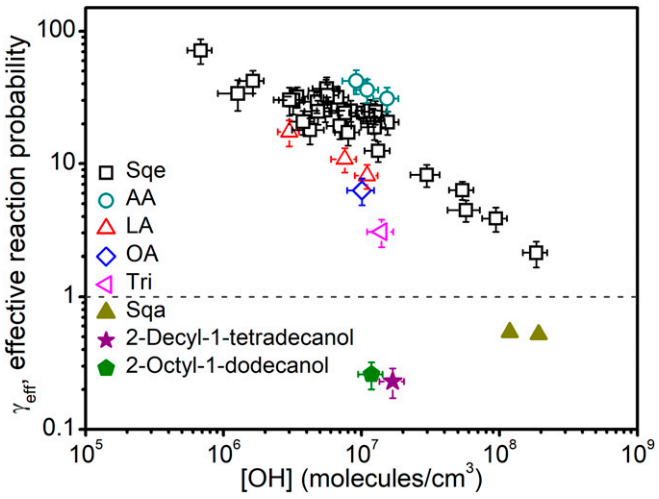

Fig. 2. Effective reaction probability (γ_{eff}) as a function of OH concentration ([OH]). γ_{eff} of Sqe, AA, LA, OA, Tri, squalane (Sqa), 2-decyl-1-tetradecanol and 2-octyl-1-dodecanol as a function of [OH] at an RH of 30%. The data for Sqa are from ref. 15. Values of $\gamma_{eff} \leq 1$ indicate that the reaction is proceeding at or below the OH collision (i.e., initiation) rate. Values larger than 1 are evidence for radical chain reactions and an overall autoxidation rate that exceeds the OH collision frequency.

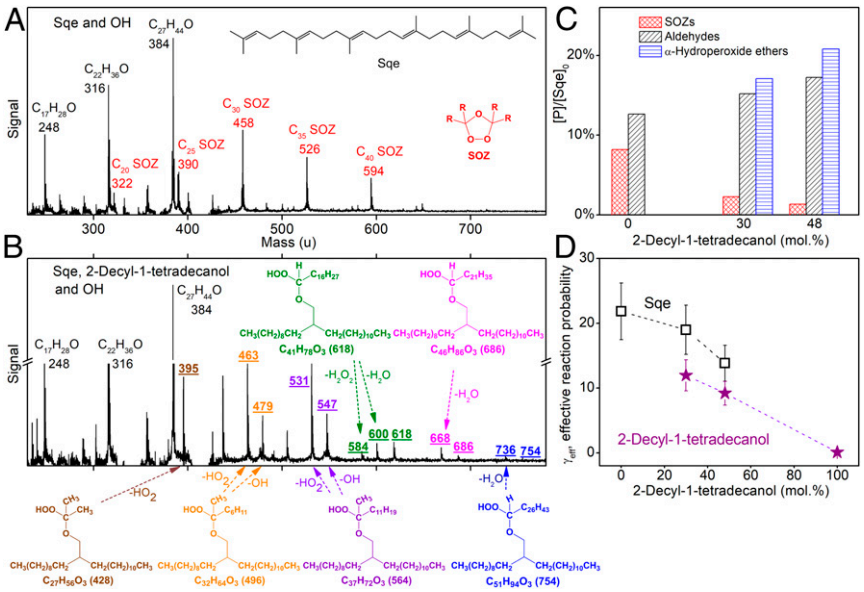

Fig. 3. (*A* and *B*) VUV-AMS of the OH + Sqe reaction products. (*C*) Reaction products and (*D*) effective reaction probability as a function of alcohol mole fraction. (*A*) Difference mass spectra (unreacted Sqe – reacted Sqe) showing aldehyde products ($C_{17}H_{28}O$, $C_{22}H_{36}O$, and $C_{27}H_{44}O$) and five SOZs. (*B*) Difference spectra showing product distribution when the CI scavenger (2-decyl-1-tetradecanol) is added to Sqe. Major products are the same three aldehydes, and six α-hydroperoxide ethers (with their structures and fragments in colors). (*C*) SOZs, aldehydes, and α-hydroperoxide ethers as a function of alcohol mole fraction (2-decyl-1-tetradecanol). (*D*) γ_{eff} of Sqe and 2-decyl-1-tetradecanol as a function of alcohol percentage (2-decyl-1-tetradecanol). All experiments are performed at [OH] (~1.2×10^7 molecules/cm^3) and under RH ~0%.

SI Appendix, Fig. S2). Alcohols are CI scavengers and upon reaction form distinctive α-hydroperoxide ether products (24). The alcohol scavengers are saturated and thus competing reactions with OH, under our reaction conditions, are very slow (Fig. 2).

As shown in Fig. 3*B*, the SOZ products disappear when adding the CI scavenger and a series of peaks form and are assigned to the expected α-hydroperoxide ether products. These products often do not appear as molecular ions but rather at *m/z* values corresponding to the elimination of either H_2O_2, HO_2, H_2O, or OH—likely due to dissociative photoionization. In separate control experiments, the same CI scavenger was used in the O_3 + Sqe reaction where CIs are known to form. The same set of peaks are observed (*SI Appendix*, Fig. S3) thus confirming the assignments in Fig. 3 for the OH reaction. The six distinct α-hydroperoxide ether products originate from the reactions (*SI Appendix*, Figs. S4 and S5) of the alcohol with the six possible CI ($C_3H_6O_2$, $C_8H_{14}O_2$, $C_{13}H_{22}O_2$, $C_{17}H_{28}O_2$, $C_{22}H_{36}O_2$, and $C_{27}H_{44}O_2$) formed in Sqe (21).

As shown in Fig. 3*C*, increasing the alcohol mole fraction decreases the quantity of SOZ, which is accompanied by a corresponding increase in aldehydes and α-hydroperoxide ether products. This is a consequence of the competition between CI + aldehyde reactions to form SOZ and CI + alcohol reactions that form α-hydroperoxide ethers.

Importantly, increasing the concentration of the CI scavenger (2-decyl-1-tetradecanol) decreases γ_{eff} (i.e., autoxidation rate) for Sqe (Fig. 3*D*). At an alcohol mole fraction of 48%, the radical chain length decreases by a factor of ~2 from a value of 21 (pure Sqe). It is accompanied by a substantial increase in the apparent γ_{eff} of the alcohol ($\gamma_{eff} > 10$ in a 30% mixture with Sqe), as it is increasingly consumed by CI formed in the reaction. Together these observations show that CI reaction pathways are central both for the formation of SOZs and α-hydroperoxide ether products as well as for controlling the overall rate of autoxidation.

An additional set of experiments reveals the general importance of CI in the OH autoxidation of cis-9-tricosene and the three unsaturated lipid acids (AA, LA, and OA). These include reactions with OH (and separate control reactions with O_3 for comparison), with and without the CI scavengers (*SI Appendix*, Figs. S6–S13). With the addition of the alcohol scavenger to pure cis-9-tricosene, α-hydroperoxide ethers products appear, thus confirming the production of CI during OH autoxidation.

For the three fatty acids, the carboxylic acid group can additionally react with CI to produce hydroperoxide esters (25). These are detected, and confirmed using separate O_3 experiments (*SI Appendix*, Figs. S8–S13). For AA, α-hydroperoxide ethers are detected with the alcohol scavenger, while without the scavenger the hydroperoxide ester is not and is a subject for future investigation.

From these measurements, we can conclude that the dominant OH-initiated autoxidation products (e.g., SOZs) arise from CI pathways, which appear also to play a central role in controlling autoxidation rates (Fig. 3*D*). These products are not explained by the established autoxidation mechanism (Fig. 1*A*). Additionally, the substantial changes in the mass spectra observed when adding alcohol or water (described below) are not consistent with the established autoxidation mechanism, since peroxy radicals (RO_2), unlike CI, do not readily react with H_2O or alcohol.

Based these observations and reported CI pathways (26–28), an autoxidation mechanism is proposed and shown in Fig. 1*B*. The initiation step involves the OH addition to the C=C bond of the lipid and subsequent O_2 addition to generate a β-hydroxyl peroxyl radical (Fig. 1*B*). This differs substantially from the established initiation step of H abstraction and is likely unique to OH (vs. other ROS). Two β-hydroxyl peroxy radicals can react to form stable termination products or alkoxy radicals. Alternatively, C–C bond scission of the β-hydroxyl peroxyl radical could produce a CI and α-hydroxyl alkyl radical, consistent with the recent results of Beauchamp and coworkers (23). In the gas phase, rapid unimolecular decomposition of the CI can regenerate OH (27). This OH, in turn, adds to another C=C bond to propagate the chain reaction. We propose that this is the key propagation step that explains the large γ_{eff} (Fig. 2) and its dependence upon C=C bond number (e.g., Sqe vs. Tri) as well as the decrease in γ_{eff} with the addition of the CI scavenger (Fig. 3).

Bimolecular reactions of CI (Fig. 1*B*) terminate the chain reaction, such as the reaction with aldehydes to produce SOZs (22), or with alcohol to produce α-hydroperoxide ethers (24), which are consistent with the mass spectra shown in Fig. 3.

Water plays a substantial role in vivo and in the environment. Hence, we examined how water impacts the autoxidation rate of Sqe. As expected (Fig. 4), the concentration of SOZs decrease with increasing relative humidity (RH), reflecting the competition between reactions of CI with water vs. aldehydes as shown in Fig. 1*B* (21). Importantly, however, γ_{eff} does not change with increasing RH, indicating that water has no apparent effect on the magnitude of the autoxidation rate. The CI + H_2O reaction produces a carbonyl product and an additional ROS species—H_2O_2 (29, 30), which is likely photolyzed to reform OH thereby sustaining the autoxidation chain reaction. In vivo or in other environments, it is likely that OH would be regenerated from H_2O_2 via other pathways involving Fenton-type chemistry.

Here we report evidence that lipid autoxidation initiated by OH is propagated by CI. This mechanism is an additional pathway to the established one (i.e., initiated by H abstraction and propagated by peroxy radicals) and is likely unique to OH. Despite the identity of the initiating ROS, the two pathways are in reality intertwined, since OH can be formed in the established mechanism either by the thermal decomposition of ROOH/H_2O_2 or by Fenton's chemistry in biological systems. This mechanism generates many of the volatile aldehyde products associated with the onset of rancidity in food products and cellular membrane decomposition. The formation of SOZ products suggests new studies are needed to evaluate their chemistry in biological environments. More generally, these results imply that CIs play a much more general role, beyond atmospheric chemistry, in the oxidative destruction of organic molecules in a variety of natural and industrial environments.

Methods

Two experimental setups are used to study the heterogeneous oxidation of lipids. For the lipid oxidation experiments using OH, a continuous flow stirred tank reactor (CFSTR) was used and is described in detail in refs. 15, 18, and 31. For oxidation experiments using ozone (O_3), a flowtube reactor is used and is described in further detail in ref. 21. Both reactors operate at atmospheric pressure and room temperature (25 °C).

Polydisperse lipid droplets are formed via the homogeneous nucleation. This is done by passing dry N_2 through a heated Pyrex tube containing the neat liquid (either lipid or lipid/alcohol mixture). Furnace temperatures are adjusted for each lipid (based upon vapor pressure) to achieve stable droplet formation. For example, 135 °C was used for Sqe and 125 °C for LA. As the flow passes out of the oven it cools, nucleating droplets (~10^6 cm^{-3}) in a log-normal distribution with an average particle diameter ~200 nm. The particle-laden flow is then passed through an annular activated charcoal denuder to remove any residual gas-phase contributions to the droplets flow. The final average nanodroplet mass concentrations introduced into the CFSTR or the flowtube reactor is ~2,000 μg/m^3. Prior to entering the reactors, the aerosol flow is combined with additional flows containing oxidant (H_2O_2 or O_3) and variable flows of humidified and dry N_2 to control the RH. A fixed flow of O_2 (0.1 standard liter per minute, SLM) is also introduced into the reactor (CFSTR or flowtube reactor).

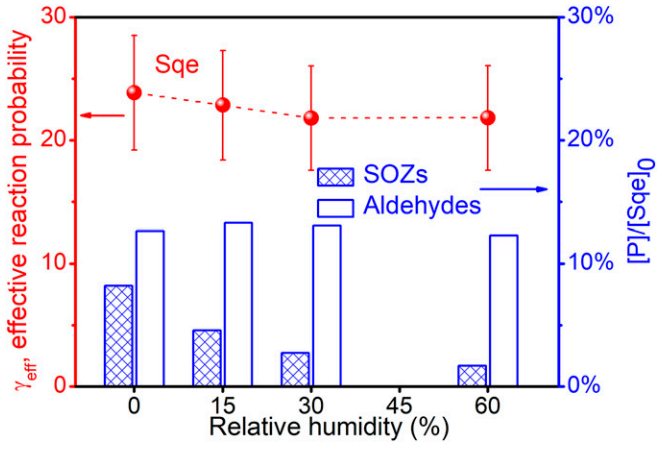

Fig. 4. Effective reaction probability (γ_{eff}) of Sqe, relative fraction of SOZs and aldehydes as a function of % RH in the Sqe + OH reaction. (Left *y* axis) γ_{eff} of Sqe and (Right *y* axis) normalized sum of the five SOZs (C_{20}, C_{25}, C_{30}, C_{35}, C_{40}) and three aldehydes ($C_{17}H_{28}O$, $C_{22}H_{36}O$, $C_{27}H_{44}O$) as a function of RH. All experiments are performed at [OH] ~1.5×10^7 molecules/cm^3. These results indicate that although the product distributions depend upon RH, the autoxidation rate does not.

For the O_3 oxidation experiments, the mixture of droplets and gases are introduced into a flowtube reactor (140 cm long and 2.5 cm inner diameter) with an average residence time of ~37 s at a total flow of 1.1 SLM. O_3 is produced by passing the 0.05-SLM O_2 through a corona discharge generator and then diluted by the dry N_2 (3 SLM). The O_3 concentration (0–10 ppm) is then measured with an ozone monitor (2B technology model 202M).

For OH oxidation in the CFSTR, OH is generated in situ by the photolysis of gas-phase H_2O_2 using two 45-cm UV lamps (blacklights, λ ~356 nm) housed inside 2.54-cm-diameter GE type 214 quartz sleeves. [OH] is controlled by adjusting the power of the UV lamps. Gaseous H_2O_2 is produced by passing the N_2 (0.1 SLM) through a heated bubbler (60 °C) containing a mixture of 50% urea-hydroperoxide ($CO[NH_2]_2{\cdot}H_2O_2$, Sigma-Aldrich, 97% pure) and 50% sand (SiO_2, 50–70 mesh particle size, Sigma-Aldrich). The final concentration of H_2O_2 in the CFSTR is <10 ppm. An additional flow containing a gas-phase tracer (such as 2-methyl-2-butene, *n*-hexane, or *n*-hexanal) is introduced into the CFSTR in order to determine the OH concentration ([OH]) using a relative rate technique as described in refs. 15, 21, and 32. The tracer concentration in the CFSTR is ~200 ppb. Additional checks with and without the tracer revealed that its presence in the reactor does not alter the overall chemistry (i.e., kinetics and product distributions). The total flow rate through the CFSTR was kept at ~1.1 SLM, yielding reaction times that span hours.

As described in detail by Che et al. (15) and reviewed briefly here, measurements in the CFSTR occur in three steps. First, prior to each experiment, the CFSTR is purged for hours with dry N_2 (~10 SLM) to eliminate particles, tracer, H_2O_2, O_2, etc. from the previous experiment. Then the reactor is filled with the fresh reagents (lipid particles, H_2O_2 gas, tracer, dry or humidified N_2, O_2) with the lamps off. After a ~2-h filling time, the lamps are turned on to initiate the reaction by photolysis of H_2O_2 to produce OH. The time evolution of the reaction is monitored by the following instruments. A gas chromatograph, equipped with a flame ionization detector (SRI Instruments 8610C), is used to monitor the decay of the gas-phase tracer to determine the [OH]. A scanning mobility particle sizer (TSI 3080L DMA and 3025A CPC) is used to measure the particle-size distribution. For example, the Sqe particle size is observed to decrease by ~5% under dry conditions and by ~10% at an RH of 60%. The chemical composition of the lipid aerosol is measured using a home-made vacuum UV aerosol mass spectrometer (VUV-AMS) located at the Chemical Dynamics Beamline (9.0.2), Advanced Light Source (ALS), Lawrence Berkeley National Laboratory, Berkeley, CA, USA. The VUV light is filtered by an argon gas filter and a MgF_2 window to remove the high harmonics produced by the undulator. To record mass spectra, lipid droplets are first vaporized at ~130 °C and then the gas phase is photoionized using VUV radiation. Variable photon energies are used for each lipid to minimize ion fragmentation: for example, 9.6 eV for Sqe and 10.2 eV for LA. This instrument has been used extensively in prior studies of heterogeneous reactions and further details can be found in refs. 19 and 32.

As described in detail in Che et al. (15), by combining the fill and decay kinetics of the OH tracer (e.g., 2-methyl-2-butene), and the fill kinetics of the particles and the mass spectral decay signal of the parent lipid compound, effective reaction probability can be quantified (Figs. 2 and 4). It is very difficult to determine the absolute concentrations of products due to the lack of photoionization cross-sections and ion fragmentation probabilities. Thus, instead the product abundance (%) is reported relative to the unreacted Sqe signal (Figs. 3 and 4). Reaction products with m/z < 200 are not shown in spectrum since it is difficult to distinguish these smaller products from ion fragments produced by the dissociative photoionization of larger species (e.g., SOZ). Additionally, these smaller products are volatile and would most likely evaporate from the aerosol (21).

Data Availability Statement. All data discussed in the paper are available in the main text and *SI Appendix*.

ACKNOWLEDGMENTS. We thank Bruce Rude for assistance at the ALS, Frances Houle, Martin Head-Gordon, Jonathan Wong, Michael I. Jacobs, and Alexander Prophet for the helpful discussions. This work was supported by Gas Phase Chemical Physics program in the Chemical Sciences Geosciences and Biosciences Division of the Office of Basic Energy Sciences of the US Department of Energy under Contract DE-AC02-05CH11231. This research used resources of the ALS, which is a US Department of Energy Scientific User Facility under Contract DE-AC02-05CH11231.

1. S. Gligorovski, R. Strekowski, S. Barbati, D. Vione, Environmental implications of hydroxyl radicals ((•)OH). *Chem. Rev.* **115**, 13051–13092 (2015).
2. W. H. Koppenol, The Haber-Weiss cycle–70 years later. *Redox Rep.* **6**, 229–234 (2001).
3. H. Yin, L. Xu, N. A. Porter, Free radical lipid peroxidation: Mechanisms and analysis. *Chem. Rev.* **111**, 5944–5972 (2011).
4. D. J. Betteridge, What is oxidative stress? *Metabolism* **49** (suppl. 1), 3–8 (2000).
5. D. Trachootham, J. Alexandre, P. Huang, Targeting cancer cells by ROS-mediated mechanisms: A radical therapeutic approach? *Nat. Rev. Drug Discov.* **8**, 579–591 (2009).
6. K. J. Barnham, C. L. Masters, A. I. Bush, Neurodegenerative diseases and oxidative stress. *Nat. Rev. Drug Discov.* **3**, 205–214 (2004).
7. K. U. Ingold, D. A. Pratt, Advances in radical-trapping antioxidant chemistry in the 21st century: A kinetics and mechanisms perspective. *Chem. Rev.* **114**, 9022–9046 (2014).
8. S. Bergstrom, Autoxidation of linoleic acid. *Nature* **156**, 717–718 (1945).
9. J. L. Bolland, Kinetics of olefin oxidation. *Q. Rev. Chem. Soc.* **3**, 1–21 (1949).
10. K. M. Schaich, "Challenges in elucidating lipid oxidation mechanisms: When, where, and how do products arise?" in *Lipid Oxidation: Challenge in Food Systems*, A. Logan, U. Nienaber, X. Q. Pan, Eds. (American Oil Chemists' Society, 2013), chap. 1, pp. 1–52.
11. M. Morita, M. Tokita, The real radical generator other than main-product hydroperoxide in lipid autoxidation. *Lipids* **41**, 91–95 (2006).
12. E. Niki, Free radical initiators as source of water- or lipid-soluble peroxyl radicals. *Methods Enzymol.* **186**, 100–108 (1990).
13. M. G. J. Heijman, A. J. P. Heitzman, H. Nauta, Y. K. Levine, A pulse radiolysis study of the reactions of OH/O^- with linoleic acid in oxygen-free aqueous solution. *Radiat. Phys. Chem. (1977)* **26**, 83–88 (1985).
14. J. Cadet, J. R. Wagner, DNA base damage by reactive oxygen species, oxidizing agents, and UV radiation. *Cold Spring Harb. Perspect. Biol.* **5**, a012559 (2013).
15. D. L. Che, J. D. Smith, S. R. Leone, M. Ahmed, K. R. Wilson, Quantifying the reactive uptake of OH by organic aerosols in a continuous flow stirred tank reactor. *Phys. Chem. Chem. Phys.* **11**, 7885–7895 (2009).
16. K. O. Johansson, M. P. Head-Gordon, P. E. Schrader, K. R. Wilson, H. A. Michelsen, Resonance-stabilized hydrocarbon-radical chain reactions may explain soot inception and growth. *Science* **361**, 997–1000 (2018).
17. K. R. Wilson *et al*., Thermal vaporization of biological nanoparticles: Fragment-free vacuum ultraviolet photoionization mass spectra of tryptophan, phenylalanine-glycine-glycine, and β-carotene. *J. Phys. Chem. A* **110**, 2106–2113 (2006).
18. N. K. Richards-Henderson, A. H. Goldstein, K. R. Wilson, Sulfur dioxide accelerates the heterogeneous oxidation rate of organic aerosol by hydroxyl radicals. *Environ. Sci. Technol.* **50**, 3554–3561 (2016).
19. C. L. Liu *et al*., The direct observation of secondary radical chain chemistry in the heterogeneous reaction of chlorine atoms with submicron squalane droplets. *Phys. Chem. Chem. Phys.* **13**, 8993–9007 (2011).
20. N. Nicolaides, Skin lipids: Their biochemical uniqueness. *Science* **186**, 19–26 (1974).
21. N. Heine, F. A. Houle, K. R. Wilson, Connecting the elementary reaction pathways of criegee intermediates to the chemical erosion of squalene interfaces during ozonolysis. *Environ. Sci. Technol.* **51**, 13740–13748 (2017).
22. R. Criegee, Mechanism of ozonolysis. *Angew. Chem. Int. Ed. Engl.* **14**, 745–752 (1975).
23. X. Zhang, K. M. Barraza, J. L. Beauchamp, Cholesterol provides nonsacrificial protection of membrane lipids from chemical damage at air-water interface. *Proc. Natl. Acad. Sci. U.S.A.* **115**, 3255–3260 (2018).
24. N. A. I. Watson, J. A. Black, T. M. Stonelake, P. J. Knowles, J. M. Beames, An extended computational study of criegee intermediate-alcohol reactions. *J. Phys. Chem. A* **123**, 218–229 (2019).
25. R. Chhantyal-Pun *et al*., Criegee intermediate reactions with carboxylic acids: A potential source of secondary organic aerosol in the atmosphere. *ACS Earth Space Chem.* **2**, 833–842 (2018).
26. C. A. Taatjes, Criegee intermediates: What direct production and detection can teach us about reactions of carbonyl oxides. *Annu. Rev. Phys. Chem.* **68**, 183–207 (2017).
27. F. Liu, J. M. Beames, A. S. Petit, A. B. McCoy, M. I. Lester, Infrared-driven unimolecular reaction of CH_3CHOO Criegee intermediates to OH radical products. *Science* **345**, 1596–1598 (2014).
28. C. A. Taatjes *et al*., Direct measurements of conformer-dependent reactivity of the Criegee intermediate CH_3CHOO. *Science* **340**, 177–180 (2013).
29. B. Long, J. L. Bao, D. G. Truhlar, Unimolecular reaction of acetone oxide and its reaction with water in the atmosphere. *Proc. Natl. Acad. Sci. U.S.A.* **115**, 6135–6140 (2018).
30. M. Kumar, D. H. Busch, B. Subramaniam, W. H. Thompson, Role of tunable acid catalysis in decomposition of α-hydroxyalkyl hydroperoxides and mechanistic implications for tropospheric chemistry. *J. Phys. Chem. A* **118**, 9701–9711 (2014).
31. N. K. Richards-Henderson, A. H. Goldstein, K. R. Wilson, Large enhancement in the heterogeneous oxidation rate of organic aerosols by hydroxyl radicals in the presence of nitric oxide. *J. Phys. Chem. Lett.* **6**, 4451–4455 (2015).
32. J. D. Smith *et al*., The heterogeneous reaction of hydroxyl radicals with sub-micron squalane particles: A model system for understanding the oxidative aging of ambient aerosols. *Atmos. Chem. Phys. Discuss.* **9**, 3945–3981 (2009).